Synchronization Driven Reciprocity Breaking

Alexander K. Stoychev,[1,*] Ulrich Kuhl,[1,2] and Nicolas Noiray[1,†]
[1]Department of Mechanical and Process Engineering, CAPS Laboratory, ETH Zürich, 8092 Zürich, Switzerland
[2]Université Côte d'Azur, CNRS, Institut de Physique de Nice (INPHYNI), 06200 Nice, France

(Received 26 July 2025; revised 23 November 2025; accepted 29 May 2026; published 16 July 2026)

Wave transmission reciprocity is broken by exploiting the synchronization of two coupled self-oscillators. The underlying principle is that illumination from one port drives the in phase, while illumination from the other port drives the antiphase synchronization state. Because of its self-adjustment the system is operationally stable. An experimental demonstration with aeroacoustic cavities is presented. They behave as weakly nonlinear limit cycles when driven by a constant airflow, leading to self-oscillations that can couple to the surrounding waveguides via two ports. Incident waves from one port trigger antiphase synchronization, causing destructive interference and low transmission, while waves from the opposite port induce in-phase synchronization, resulting in high transmission. This directional dependence effectively breaks reciprocity, where the operational bandwidth is defined by the synchronization region and can be broader than resonance-based methods. Experimental results show robust nonreciprocal behavior with respect to parameter changes. Moreover, a modified temporal coupled mode theory is proposed, explaining the system's nonlinear dynamics and scattering properties in a quantitative manner. This synchronization-based approach offers a new avenue for directional wave control, complementing traditional reciprocity breaking techniques and offering an intrinsic loss compensation emanating from the self-oscillation of meta-atoms.

DOI: 10.1103/jln4-jg5c

Introduction—Lorentz reciprocity in passive linear wave media dictates that source and receiver are interchangeable under the assumptions of (microscopic) time-reversal symmetry and time invariance, implying that an unidirectional transmission (e.g., diodes, insulators, circulators, etc.) requires bias or nontrivial material properties. In particular, strategies to break reciprocity have been characterized [1] into (i) momentum bias (breaking time reversibility) [2–9], (ii) spatiotemporal modulations (breaking time invariance) [10–28], and (iii) structural asymmetry with nonlinearity (breaking linearity) [29–36]. To achieve nonreciprocity in kinetic medium, a momentum bias could be introduced via magnetic fields [2], spinning masses [3,4], Coriolis forces [5], circulating fluids [6], "tilted" band structures [7], and drifting electrons [8], although time reversibility could also be broken via wave-vector modulation [9]. Conversely, spatiotemporal modulations can break time invariance through one-way mode conversion [11,12], frequency conversion [13,14], synthetic motion [15], anomalous Doppler effects [16–18], nonreciprocal Willis coupling [19–24], topologically protected edge states [25–28], etc. Finally, reciprocity breaking nonlinear effects could range from generation of harmonics and bandpass filtering [29,30] to quasibound states in a continuum [31], frequency conversion in a multimode system [32], bifurcation driven transitions [34], static response of an asymmetric structure [35], self-demodulation effects [37], or topological solitons [38].

We propose a fundamentally different approach, which relies on weakly nonlinear self-oscillators and direction-dependent synchronization processes rather than bias, spatiotemporal modulation, band topology, or conventional nonlinearity. In particular, the self-oscillator (SO) here denotes an autonomous, saturable-gain element, whose individual steady state is a stable limit cycle emitting a single dominant frequency, which can be phase and frequency locked by an external drive inside a subset of amplitude-frequency space (i.e., the synchronization region or Arnold tongue, Chap. 3.1.2 [39]). Consequently, when two SOs are coupled to the same waveguide ports, the scattering behavior is governed by the relative phase of the locked limit cycles (Fig. 1). Specifically, since opposite injection ports can favor different synchronization branches (in phase or antiphase), waves incident from opposite directions experience dramatically different transmission, i.e., destructive interference in one direction [Fig. 1(a)], yet not in the other [Fig. 1(b)]. The resulting synchronization

*Contact author: astoychev@ethz.ch
†Contact author: noirayn@ethz.ch

Published by the American Physical Society under the terms of the Creative Commons Attribution 4.0 International license. Further distribution of this work must maintain attribution to the author(s) and the published article's title, journal citation, and DOI.

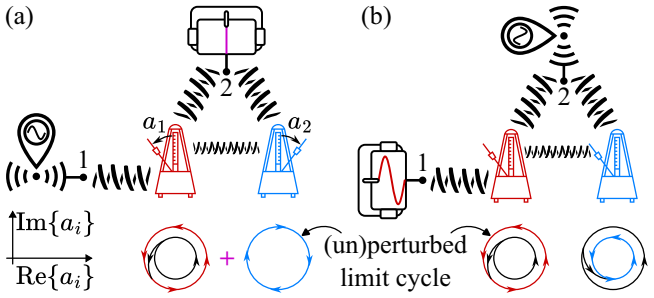


FIG. 1. Principle of the synchronization driven reciprocity breaking. (a) Incidence from port 1 couples to one of the limit cycles (red) and due to the nonlinear interaction of the self-oscillators, both contribute to the transmission. (b) Incidence from port 2 forces both SOs simultaneously, while only the red SO determines the transmission. The direct coupling between the ports is weak by design; consequently, the (forced) synchronization state governs the scattering properties of the system. The lower part indicates phase-space transition of the limit cycles upon incidence from the outside.

pattern governs the reciprocity breaking, where the bandwidth is set by the width of the joint synchronization region, while the weak nonlinearity filters out small perturbations. Crucially, the two SOs do not need to be precisely adjusted. It is sufficient that the driving frequency-amplitude pair is in the range of the joint synchronization region, and importantly, the SOs lock to the injected signal; hence, frequency shifts are avoided. This mechanism is generic to systems supporting weakly nonlinear limit cycles and is compatible with the modified temporal coupled mode theory (TCMT) developed below, where additional technical details can be found in Supplemental Material [40] and in Ref. [42].

Note that synchronization driven strategies generally avoid transferring energy into different spectral channels, which is common to conventional methods such as momentum bias (e.g., [6–9]), spatiotemporal modulations (e.g., [12–15]), or nonlinearity (e.g., [29–32]). Furthermore, the proposed synchronization-based scattering employing interconnected self-oscillators also displays essential differences to synchronization techniques rooted in any of the aforementioned mechanisms, such as the Zeeman-type mode splitting approach in [43] that builds on [6]. Specifically, our system depends robustly on the topology of the self-oscillator network, thus guiding the flow of energy through particular routes in phase space and allowing us to suppress transmission over a range of incident amplitudes, while simultaneously permitting tunable forward behavior (lossy, unitary, or superradiant). In contrast, the system in [43] produces near-zero transmission to the isolated port only at a specific incident amplitude and bias. Moreover, because the former manipulates the state of distinct oscillators, it readily transfers to platforms where introducing bias might be impractical (e.g., microwave graphs, elastic networks, coupled optical cavities, etc).

Results—In the following, we focus on an aeroacoustic implementation (Fig. 2) of a two port system based on the synchronization approach discussed above. Specifically, a limit cycle is implemented through a self-oscillating cavity mode, pumped by the self-induced conversion of an externally supplied, steady flow's kinetic energy into an acoustic one [42]. Note that, in this case, the underlying mode derives from the constant pressure solution of a rigid cavity and, therefore, is (i) incommensurate with any higher order eigenfrequencies and (ii) resulting in a large wavelength compared to the dimensions of the meta-atom. Nevertheless, those properties are not essential to the proposed method and we could consider noncompact scatterers by working with higher order modes of the whistle, taking advantage of π phase shifts at different port locations. Crucially, however, the response is only weakly nonlinear and nonreciprocity is achieved at the frequency of the incident wave. Consequently, over the frequency range of interest, each whistle behaves as a single-degree-of-freedom self-oscillator with a dominant fundamental component and negligible spectral weight in higher harmonics, which justifies asymptotic averaging [44] and leads to the set of first order nonlinear ordinary differential equations for the complex amplitudes $a_{1\{2\}}$ we derive below.

The limit cycles are coupled to the surrounding waveguides (and each other) via small perforations in the cavity side walls, which allows them to synchronize with the incident wave and with each other (Fig. 2). Since the resonant coupling (no limit cycle) is weak enough to render the individual oscillators mostly reflective [42], the scattering properties are determined by the synchronization state of the system. The latter can be tuned by the distance between the whistles, which corresponds to the coupling phase of the SOs. Moreover, varying the position of the source could result in (i) the self-sustained antiphase mode being excited by manipulating the synchronization phase of the first oscillator via the first port, leading to phase canceling and low transmission [Fig. 1(a)] or to (ii) the in-phase mode being instigated by forcing both oscillators to synchronize with a wave incident from the second port, leading to high transmission [Fig. 1(b)]. Analogous to the scattering by a single element [42], the latter can exhibit (i) lossy, (ii) unitary, or (iii) superradiant behavior.

Note that the synchronized states we are interested in are constrained to specific regions in parameter space, concretely, the ones where the incident amplitude is large enough compared to the frequency detuning (interior of the Arnold tongue). Inside the aforementioned areas, the spectrum of the resulting signal is nearly monochromatic (fundamental frequency-based total harmonic distortion $< 10^{-4}$), where outside thereof we find at least two significant components: (i) at the self-oscillation in addition to (ii) the omnipresent incident frequency, with (iii) even richer response close to synchronization (cf. [42], Appendix B).

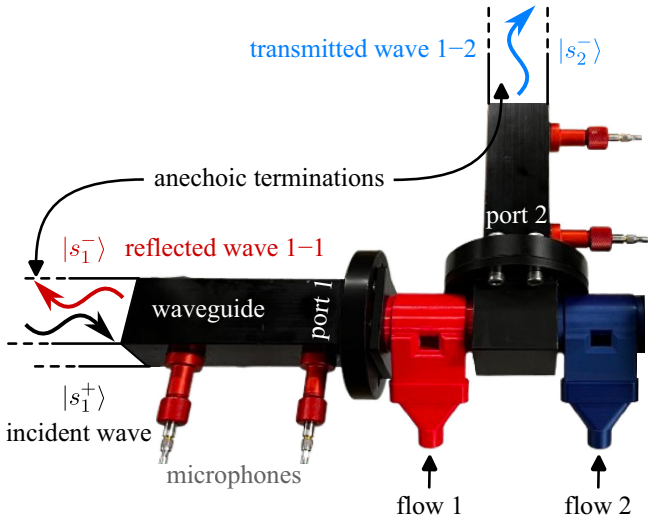


FIG. 2. Aeroacoustical implementation of the reciprocity breaking self-excited meta-atom assembly. Only an incidence from port 1 is depicted here, where an incidence from port 2 follows analogously (cf. Fig. 1). The apertures on top of the cavities add irreversible losses in the passive case (no limit cycle) and saturable gain in the self-excited case (limit cycle). The whistles are coupled to the waveguides via small perforations on the sides, where the second (fed by flow 2) is coupled only to port 2, enabling the needed phase-space routing. Note that there is no further port on the right.

Experimental measurements—Figure 3 illustrates the concept, where the four subpanels depict the corresponding entries of the scattering matrix, each as a function of the incident wave's frequency and amplitude.

In particular, comparison between the transmission from port 1 to port 2 (S_{21}) and the reverse (S_{12}), i.e., the off-diagonal elements, shows the expected unidirectional channeling close to the self-oscillation frequency ($f_0 \approx 1187$ Hz). Although the scattering properties of the system are intrinsically affected by the incident amplitude due to nonlinear effects [42], this dependence is relatively weak, leading to a comparatively robust to perturbations reciprocity breaking mechanism. Specifically, over the considered range, we observe slightly superradiant transmission in one direction ($S_{12} > 1$) and (approximate) phase canceling in the other ($S_{21} \approx 0$), where the bandwidth of the former is inherited from the Arnold tongue [42] and the one of the latter is determined by the phase relations of the synchronization state.

Note that, given a detuning and coupling strength, fundamentally and irrespectively of implementation, there exists a minimum incident amplitude above which the two oscillators lock to the injected frequency and settle on either the in-phase or antiphase synchronization branch. The branch selection depends on coupling and injection port, the frequency detuning determines the synchronization phases, and the incident amplitude primarily rescales the magnitude of the scattering coefficients. Consequently, unlike synchronization-based biased circulators that produce near-zero transmission only at a single incident amplitude and bias pair [43], the synchronization-based scattering employed here robustly depends on the topology of the self-oscillator network. It can suppress transmission over a range of incident amplitudes that fall inside the joint synchronization region of the coupled limit cycles, while simultaneously enabling tunable forward transmission (cf. Fig. 3).

Theoretical model—To model the experimentally observed behavior, we adopt a TCMT approach [45], although, with several necessary modifications (cf. [40]), i.e.,

$$\frac{\mathrm{d}a_1}{\mathrm{d}\tau} = \left(j\frac{1-\Omega^2}{2\Omega} + \frac{\mu}{2}\frac{1-|a_1|^2}{1+|a_1|^2}\right)a_1 - \varkappa a_2 + \langle\kappa_1|s^+\rangle, \tag{1}$$

$$\frac{\mathrm{d}a_2}{\mathrm{d}\tau} = \left(j\frac{1-\Omega^2}{2\Omega} + \frac{\mu}{2}\frac{1-|a_2|^2}{1+|a_2|^2}\right)a_2 - \varkappa a_1 + \langle\kappa_2|s^+\rangle, \tag{2}$$

$$|s^-\rangle = \mathbf{D}|s^+\rangle + |\tilde{\kappa}_1\rangle a_1 + |\tilde{\kappa}_2\rangle a_2, \tag{3}$$

where $\mathrm{d}/\mathrm{d}\tau$ represents derivative with respect to time, normalized by the self-oscillation frequency ($f_0 \in \mathbb{R}$), while j denotes the imaginary unit, and $\Omega = f/f_0 \in \mathbb{R}$ is the ratio between intrinsic ($1/f_0$) and forcing timescale ($1/f$). Furthermore, $a_{1\{2\}} \in \mathbb{C}$ characterizes the complex amplitude of the corresponding limit cycle, with $|a_{1\{2\}}|$ and $\arg\{a_{1\{2\}}\}$ describing the slow timescale magnitude and phase behavior, respectively. Moreover, $\mu \in \mathbb{R}$ incorporates the radiation and viscous losses and $\varkappa = |\kappa_1||\tilde{\kappa}_2|\exp(j\phi) = |\kappa_2||\tilde{\kappa}_1|\exp(j\phi) \in \mathbb{C}$ relates to the inter-limit-cycle interactions. Conversely, $\langle\kappa_1| = \kappa_1\langle 1| + \kappa_1\langle 2|$ and $\langle\kappa_2| = \kappa_2\langle 2|$, with $\kappa_{1\{2\}} \in \mathbb{R}$, stand for the direct coupling vectors, where $\langle 1|$ and $\langle 2|$ are the unit vectors (1,0) and (0,1), respectively. Additionally, $|s^+\rangle = s|1\{2\}\rangle$ indicates the incident wave, with $s = ||s_p^+\rangle|/|p_p| \in \mathbb{R}$ being the amplitude of the physical wave, $||s_p^+\rangle|$, normalized by the unperturbed limit cycle pressure $|p_p|$. Finally, the complex valued $\mathbf{D} \approx \mathbf{1}$ signifies the scattering matrix of the direct process and $\langle\tilde{\kappa}_1| = \tilde{\kappa}_1\langle 1| + \tilde{\kappa}_1\langle 2|$ and $\langle\tilde{\kappa}_2| = \tilde{\kappa}_2\langle 2|$, with $\tilde{\kappa}_{1\{2\}} \in \mathbb{R}$, denote the conjugate coupling vectors.

Analogous to the single limit cycle description [42], Eqs. (1)–(3) are (i) unfolding in a time-dependent reference frame, (ii) containing terms deviating from classical TCMT [45] and its nonlinear extensions [43,46,47], and (iii) breaking Lorentz reciprocity [48]. Specifically, the oscillator equations (1) and (2) originate from an asymptotic averaging of a second order Liénard-type model for the pressure [42] and, therefore, (i) represent a slow timescale evolution in a coordinate system moving in phase with the incident wave, i.e., $|s^+\rangle = |1\{2\}\rangle s$, $s = \text{const}$. Consequently, (ii) asymmetric detuning terms

$j(1-\Omega^2)/2\Omega$ and multiplicative forcing factors $j/2\Omega$ follow. Finally, (iii) the coupling terms between incident wave and self-oscillator are assumed to depend on the direction of the energy flow [$\kappa \neq \tilde{\kappa}$] due to nonlinear effects. Note that since the primitive physical description is averaged with respect to a harmonic incident wave (c.f. [40]), we chose $s = ||s^+\rangle|$ as the measure of "amplitude," although other definitions, e.g., $s_{\mathrm{rms}} = s/\sqrt{2}$, are often used in acoustics.

The aforementioned considerations are required to adequately describe the physical phenomenon we observe, however, some further simplifications could be attempted. Specifically, the individual coefficients of the two oscillators [$f_{0,i}$, μ_i, κ_i, $\tilde{\kappa}_i$, and $\varkappa$] could be, and in practice are, independent; however, imposing the simplifying assumptions $f_{0,1} = f_{0,2} = f_0$, $\mu_1 = \mu_2 = \mu$, and $|\varkappa| = |\kappa_1||\tilde{\kappa}_2|$ could still be useful. Indeed, those approximations are justified, since the two whistles are nearly identical and operated at closely matched flow rates, hence, their natural frequencies and linear loss and gain parameters differ only slightly. Additionally, this simplifies the discussion of the observed behavior below. Nevertheless, retaining a small coupling asymmetry is necessary to reproduce the experimentally observed jumps and bandwidth changes, thus isolating the essential synchronization features from secondary details.

In particular, Fig. 4 shows a comparison between experimental data (markers) and Eqs. (1)–(3), where the visualized trajectory through parameter space corresponds to an incident amplitude slightly varying with frequency due to reflections from the terminations (3D lines Fig. 3). Solid and dotted lines depict solutions with independent ($\kappa_2 = 1.133\kappa_1$, $\tilde{\kappa}_2 = 1.133\tilde{\kappa}_1$) and identical ($\kappa_1 = \kappa_2 = \kappa$,

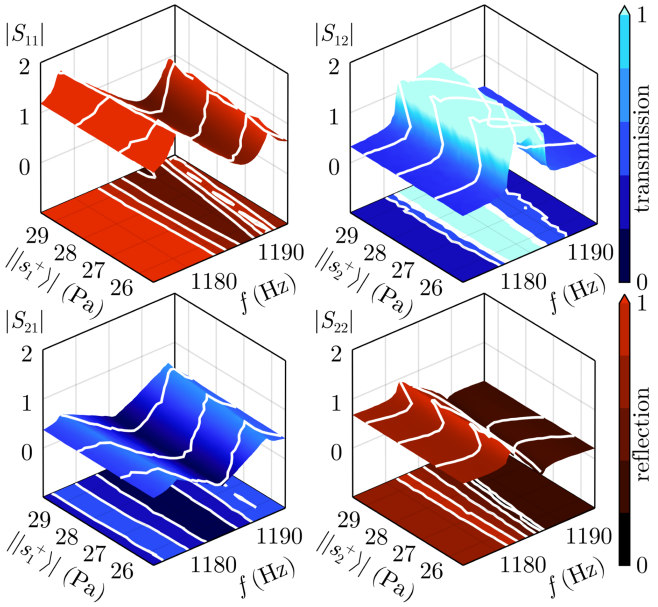


FIG. 3. Experimental measurements of the transmissions (off diagonal; S_{12} and S_{21}) and reflections (diagonal; S_{11} and S_{22}) as function of incident frequency f and amplitude $||s^+\rangle|$, for an incidence from port 1 (left; S_{11} and S_{21}) and port 2 (right; S_{12} and S_{22}), at flow rates of $\dot{Q}_1 = 11$ and $\dot{Q}_2 = 11.25$l/ min for the red and blue whistle (see Fig. 2), respectively. The scattering data show only slight dependence on the incident wave amplitude, signifying a weak nonlinearity and leading to persistent reciprocity breaking across the considered range. Conversely, the frequency f has strong effect on the reflection and a less prominent, yet significant, effect on the transmission. The bandwidth of the process is governed by the synchronization region, which can be influenced, e.g., by adjusting the coupling coefficients. Note that a loudspeaker input signal varying solely in frequency results in some incident amplitude variation due to reflections from the terminations (white lines in 3D plot). Approximate values for the scattering coefficients can be deduced from the contour plots projected below the 3D surfaces above, while exact values can be read from the 2D sections depicted in Fig. 4.

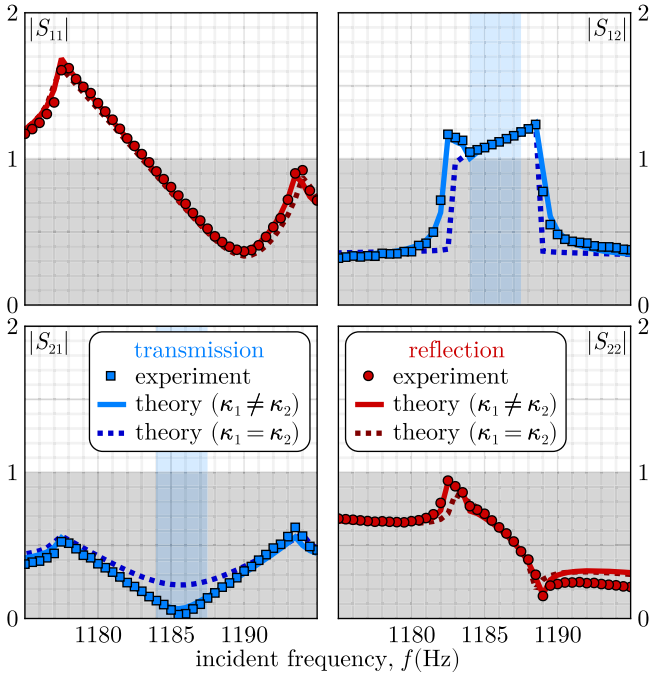


FIG. 4. Scattering coefficients as a function of frequency f for an incident amplitude of $||s_1^+\rangle| \approx ||s_2^+\rangle| \approx 29$ Pa and flow rates of $\dot{Q}_1 = 11$ and $\dot{Q}_2 = 11.25$l/ min, respectively. Left panels refer to incidence from port 1 (S_{11} and S_{21}), while right panels correspond to waves incident from port 2 (S_{21} and S_{22}; cf. Fig. 2). Blue colors represent transmission, with square markers depicting measurement points and solid (dotted) lines the theoretical calculations. Conversely, red colors denote reflection, with circular markers being measurements and solid (dotted) lines the solutions of Eqs. (1)–(3). Dotted lines correspond to $\kappa_2 = \kappa_1 = \kappa$ and solid ones to $\kappa_2 = 1.133\kappa_1$, where the latter is shown to be responsible for the transmission jump and bandwidth widening in S_{12}. Despite keeping the external excitation within each dataset constant, the actual incident amplitude varies slightly with frequency due to backreflections from the terminations (cf. 3D lines in Fig. 3). Therefore, the results (theoretical and experimental) depict a flat projection of curved trajectories through parameter space.

TABLE I. Reduced model parameters.

$\lvert p_p\rvert$ (Pa)	f_0 (Hz)	D_{11}	D_{21}	D_{12}	D_{22}	μ	$\tilde{\kappa}$	κ	$\arg \varkappa$ (rad)
350	1186.9	$0.917 \times e^{2.61j}$	$0.073 \times e^{-0.01j}$	$0.043 \times e^{0.92j}$	$0.763 \times e^{2.49j}$	0.134	0.074	0.204	−0.063

$\tilde{\kappa}_1 = \tilde{\kappa}_2 = \tilde{\kappa}$) coupling coefficients, respectively, and the model parameters are reported in Table I. Note that most details, including the jumps in S_{12} and S_{22} at $f = 1184$ Hz, are well captured by allowing $\kappa_1 \neq \kappa_2$, yet, even with the simplification $\kappa_1 = \kappa_2 = \kappa$, the main features of the synchronization driven process are quantitatively represented. For the sake of completeness, the corresponding figure for the phases of the S-matrix elements are presented in Supplemental Material [40]. Furthermore, the state of interest (Fig. 4; blue shaded region) can be roughly estimated in simpler terms by the zeroth order expansion

$$\mathbf{S} \approx \mathbf{D} + \frac{\tilde{\kappa}}{s\sqrt{\vartheta}} \begin{bmatrix} 1 & \vartheta \\ 0 & 2\vartheta \end{bmatrix}, \qquad \vartheta = \frac{\mu + 2\mathrm{Re}(\varkappa)}{\mu - 2\mathrm{Re}(\varkappa)}, \quad (4)$$

where $\mathbf{D} \approx \mathbf{1}$, and the root corresponds to the unperturbed amplitude of the in-phase mode, $|a_1| = |a_2| = |a_0^+|$, or the inverse of the antiphase one, $|a_0^+| = 1/|a_0^-|$. Crucially, $S_{21} \approx 0$ due to superposition of antiphase sources, while $S_{12} \approx |a_0^+|\tilde{\kappa}/s$. Note that (i) for $s \to 0$ and $\Omega = 1$ the scattering matrix exhibits a singularity due to $|a_{1\{2\}}| \sim \mathcal{O}(1)$, (ii) for $\tilde{\kappa} \to 0$ the direct process governs the behavior $\mathbf{S} = \mathbf{D} \approx \mathbf{1}$, and (iii) for $\varkappa \to 0$ the phase difference between the whistles is undetermined and S_{21} fluctuates without reaching a steady state.

Conclusion—Above, we have demonstrated that by utilizing the universal phenomenon of synchronization in weakly nonlinear limit cycle oscillators, we can break acoustic reciprocity in a manner that is both robust and tunable. Since the aforementioned mechanism depends only on the existence of coupled self-oscillators, it is generally independent of the specific physical implementation. Indeed, the same principles that govern the injection locking of microwave oscillators [49,50] (e.g., a dc-biased Gunn diode locking to an rf input) apply equally to our aeroacoustic whistles. In both cases, a dc-like bias establishes an autonomous oscillation, which can then be phase and frequency locked by an external drive within the synchronization region (Arnold tongue) in parameter space [51–53]. Moreover, synchronization-based methods have been shown to transcend specific fields, e.g., by a direct parallel between a phonon [54] and microwave [55] laser. Therefore, in all domains supporting self-sustained oscillations, a synchronization driven diode should be implementable by appropriately arranging the coupling and phase relations of its limit cycles. In conclusion, the presented synchronization-based paradigm may enable a new class of nonreciprocal devices across the electromagnetic, mechanical, and acoustic domains, with the potential of complementing classical resonance-based methods with intrinsic loss compensation and straightforward reconfigurability through control of pumping and coupling parameters.

Data availability—The data that support the findings of this article are openly available [56].

[1] H. Nassar, B. Yousefzadeh, R. Fleury, M. Ruzzene, A. Alù, C. Daraio, A. N. Norris, G. Huang, and M. R. Haberman, Nonreciprocity in acoustic and elastic materials, Nat. Rev. Mater. **5**, 667 (2020).

[2] C. Kittel, Interaction of spin waves and ultrasonic waves in ferromagnetic crystals, Phys. Rev. **110**, 836 (1958).

[3] L. M. Nash, D. Kleckner, A. Read, V. Vitelli, A. M. Turner, and W. T. Irvine, Topological mechanics of gyroscopic metamaterials, Proc. Natl. Acad. Sci. U.S.A. **112**, 14495 (2015).

[4] C. P. Wiederhold, D. L. Sounas, and A. Alù, Nonreciprocal acoustic propagation and leaky-wave radiation in a waveguide with flow, J. Acoust. Soc. Am. **146**, 802 (2019).

[5] T. Kariyado and Y. Hatsugai, Manipulation of dirac cones in mechanical graphene, Sci. Rep. **5**, 18107 (2015).

[6] R. Fleury, D. L. Sounas, C. F. Sieck, M. R. Haberman, and A. Alù, Sound isolation and giant linear nonreciprocity in a compact acoustic circulator, Science **343**, 516 (2014).

[7] Y. del Valle Inclan Redondo, X. Xu, T. C. Liew, E. A. Ostrovskaya, A. Stegmaier, R. Thomale, C. Schneider, S. Dam, S. Klembt, S. Höfling *et al.*, Non-reciprocal band structures in an exciton–polariton floquet optical lattice, Nat. Photonics **18**, 548 (2024).

[8] M. Liu, S. Yang, W. Chen, J. Zhou, C. Zhao, and C.-W. Qiu, Nonreciprocal thermal fizeau drag radiation around asymmetric exceptional points, Phys. Rev. Lett. **135**, 126902 (2025).

[9] Y. Hu, Y. Li, Y. Liu, B. Li, and J. Christensen, Giant elastic-wave asymmetry in a linear passive circulator, Nat. Commun. **16**, 3991 (2025).

[10] D. L. Sounas and A. Alù, Non-reciprocal photonics based on time modulation, Nat. Photonics **11**, 774 (2017).

[11] M. B. Zanjani, A. R. Davoyan, A. M. Mahmoud, N. Engheta, and J. R. Lukes, One-way phonon isolation in acoustic waveguides, Appl. Phys. Lett. **104**, 081905 (2014).

[12] Z. Yu and S. Fan, Complete optical isolation created by indirect interband photonic transitions, Nat. Photonics **3**, 91 (2009).

[13] B.-I. Popa and S. A. Cummer, Non-reciprocal and highly nonlinear active acoustic metamaterials, Nat. Commun. **5**, 3398 (2014).

[14] R. Tirole, S. Vezzoli, D. Saxena, S. Yang, T. Raziman, E. Galiffi, S. A. Maier, J. B. Pendry, and R. Sapienza, Second harmonic generation at a time-varying interface, Nat. Commun. **15**, 7752 (2024).
[15] A. Harwood, S. Vezzoli, T. Raziman, C. Hooper, R. Tirole, F. Wu, S. Maier, J. Pendry, S. Horsley, and R. Sapienza, Space-time optical diffraction from synthetic motion, Nat. Commun. **16**, 5147 (2025).
[16] X. Hu, Z. Hang, J. Li, J. Zi, and C. T. Chan, Anomalous doppler effects in phononic band gaps, Phys. Rev. E **73**, 015602 (2006).
[17] D.-W. Wang, H.-T. Zhou, M.-J. Guo, J.-X. Zhang, J. Evers, and S.-Y. Zhu, Optical diode made from a moving photonic crystal, Phys. Rev. Lett. **110**, 093901 (2013).
[18] Y. Wang, B. Yousefzadeh, H. Chen, H. Nassar, G. Huang, and C. Daraio, Observation of nonreciprocal wave propagation in a dynamic phononic lattice, Phys. Rev. Lett. **121**, 194301 (2018).
[19] H. Nassar, H. Chen, A. Norris, M. Haberman, and G. Huang, Non-reciprocal wave propagation in modulated elastic metamaterials, Proc. R. Soc. A **473**, 20170188 (2017).
[20] H. Nassar, X. Xu, A. Norris, and G. Huang, Modulated phononic crystals: Non-reciprocal wave propagation and willis materials, J. Mech. Phys. Solids **101**, 10 (2017).
[21] L. Quan, D. L. Sounas, and A. Alù, Nonreciprocal willis coupling in zero-index moving media, Phys. Rev. Lett. **123**, 064301 (2019).
[22] Y. Liu, Z. Liang, J. Zhu, L. Xia, O. Mondain-Monval, T. Brunet, A. Alù, and J. Li, Willis metamaterial on a structured beam, Phys. Rev. X **9**, 011040 (2019).
[23] W. Cheng and G. Hu, Acoustic skin effect with non-reciprocal willis materials, Appl. Phys. Lett. **121**, 041701 (2022).
[24] L. Wang, J. A. I. Martínez, G. Ulliac, B. Wang, V. Laude, and M. Kadic, Non-reciprocal and non-Newtonian mechanical metamaterials, Nat. Commun. **14**, 4778 (2023).
[25] H. Nassar, H. Chen, A. N. Norris, and G. L. Huang, Quantization of band tilting in modulated phononic crystals, Phys. Rev. B **97**, 014305 (2018).
[26] H. Chen, L. Y. Yao, H. Nassar, and G. L. Huang, Mechanical quantum Hall effect in time-modulated elastic materials, Phys. Rev. Appl. **11**, 044029 (2019).
[27] Z. Zhang, P. Delplace, and R. Fleury, Superior robustness of anomalous non-reciprocal topological edge states, Nature (London) **598**, 293 (2021).
[28] Z. Zhang, P. Delplace, and R. Fleury, Anomalous topological waves in strongly amorphous scattering networks, Sci. Adv. **9**, eadg3186 (2023).
[29] B. Liang, B. Yuan, and J.-c. Cheng, Acoustic diode: Rectification of acoustic energy flux in one-dimensional systems, Phys. Rev. Lett. **103**, 104301 (2009).
[30] B. Liang, X. Guo, J. Tu, D. Zhang, and J. Cheng, An acoustic rectifier, Nat. Mater. **9**, 989 (2010).
[31] M. Cotrufo, A. Cordaro, D. L. Sounas, A. Polman, and A. Alù, Passive bias-free non-reciprocal metasurfaces based on thermally nonlinear quasi-bound states in the continuum, Nat. Photonics **18**, 81 (2024).
[32] S. Pontula, S. Vaidya, C. Roques-Carmes, S. Z. Uddin, M. Soljačić, and Y. Salamin, Non-reciprocal frequency conversion in a non-Hermitian multimode nonlinear system, Nat. Commun. **16**, 7544 (2025).
[33] X. Guo, H. Lissek, and R. Fleury, Observation of non-reciprocal harmonic conversion in real sounds, Commun. Phys. **6**, 93 (2023).
[34] N. Boechler, G. Theocharis, and C. Daraio, Bifurcation-based acoustic switching and rectification, Nat. Mater. **10**, 665 (2011).
[35] C. Coulais, D. Sounas, and A. Alu, Static non-reciprocity in mechanical metamaterials, Nature (London) **542**, 461 (2017).
[36] Z. Lu and A. N. Norris, Non-reciprocal wave transmission in a bilinear spring-mass system, J. Vib. Acoust. **142**, 021006 (2020).
[37] T. Devaux, V. Tournat, O. Richoux, and V. Pagneux, Asymmetric acoustic propagation of wave packets via the self-demodulation effect, Phys. Rev. Lett. **115**, 234301 (2015).
[38] J. Veenstra, O. Gamayun, X. Guo, A. Sarvi, C. V. Meinersen, and C. Coulais, Non-reciprocal topological solitons in active metamaterials, Nature (London) **627**, 528 (2024).
[39] A. Pikovsky, M. Rosenblum, and J. Kurths, *Synchronization: A Universal Concept in Nonlinear Science*, Cambridge Nonlinear Science Series No. 12 (Cambridge University Press, Cambridge, England, 2001).
[40] See Supplemental Material at http://link.aps.org/supplemental/10.1103/jln4-jg5c for the phase of the scattering matrix elements and the TCMT derivation, which includes Ref. [41].
[41] A. K. Stoychev, T. Pedergnana, and N. Noiray, Synchronization under saturable nonlinearity, Chaos **34**, 081102 (2024).
[42] A. K. Stoychev, X. Guo, U. Kuhl, and N. Noiray, Synchronization driven acoustics: The nonlinear scattering of a self-oscillating meta-atom, Phys. Rev. E **113**, 044214 (2026).
[43] T. Pedergnana, A. Faure-Beaulieu, R. Fleury, and N. Noiray, Loss-compensated non-reciprocal scattering based on synchronization, Nat. Commun. **15**, 7436 (2024).
[44] N. M. Krylov and N. N. Bogoliubov, *Introduction to Non-Linear Mechanics* (Princeton University Press, Princeton, NJ, 1950).
[45] S. Fan, W. Suh, and J. D. Joannopoulos, Temporal coupled-mode theory for the Fano resonance in optical resonators, J. Opt. Soc. Am. A **20**, 569 (2003).
[46] T. Pedergnana and N. Noiray, Superradiant scattering by a limit cycle, Phys. Rev. Appl. **20**, 034068 (2023).
[47] T. Pedergnana, J. Kölliker, L. Perniola, and N. Noiray, Cloaking obstacles using synchronization, Phys. Rev. B **111**, 035427 (2025).
[48] Z. Zhao, C. Guo, and S. Fan, Connection of temporal coupled-mode-theory formalisms for a resonant optical system and its time-reversal conjugate, Phys. Rev. A **99**, 033839 (2019).
[49] B. Perlman and T. Walsh, Criterion for nonreciprocal injection locking of bilateral microwave oscillators (correspondence), IEEE Trans. Microwave Theory Tech. **18**, 507 (1970).
[50] K. Kurokawa, Injection locking of microwave solid-state oscillators, Proc. IEEE **61**, 1386 (1973).

[51] Y. Li, W. Luo, Z. Zhao, and D. Liu, Resonant excitation-induced nonlinear mode coupling in a microcantilever resonator, Phys. Rev. Appl. **17**, 054015 (2022).

[52] D. Navarro-Urrios, G. Arregui, M. F. Colombano, J. Jaramillo-Fernández, A. Pitanti, A. Griol, L. Mercadé, A. Martínez, and N. E. Capuj, Giant injection-locking bandwidth of a self-pulsing limit-cycle in an optomechanical cavity, Commun. Phys. **5**, 330 (2022).

[53] M. Euler, Universal synchronization: Acoustic experiments, the phase oscillator model and mechanical analogues, Eur. J. Phys. **45**, 023003 (2024).

[54] S. Knünz, M. Herrmann, V. Batteiger, G. Saathoff, T. W. Hänsch, K. Vahala, and T. Udem, Injection locking of a trapped-ion phonon laser, Phys. Rev. Lett. **105**, 013004 (2010).

[55] N. T. Otterstrom, S. Gertler, Y. Zhou, E. A. Kittlaus, R. O. Behunin, M. Gehl, A. L. Starbuck, C. M. Dallo, A. T. Pomerene, D. C. Trotter, A. L. Lentine, and P. T. Rakich, Backscatter-immune injection-locked Brillouin laser in silicon, Phys. Rev. Appl. **14**, 044042 (2020).

[56] https://polybox.ethz.ch/index.php/s/FtkH34XDSyiT5L5.